Parallel-Tempering Monte Carlo Study of $(H_2O)_{n\,=\,6-9}$

Arnold N. Tharrington[†] **and Kenneth D. Jordan***

Department of Chemistry and Center for Molecular and Materials Simulations, University of Pittsburgh, Pittsburgh, Pennsylvania 15260

Received: March 20, 2003; In Final Form: June 5, 2003

Parallel-tempering Monte Carlo simulations are used to characterize the finite temperature behavior of the $(H_2O)_{n\,=\,6-9}$ clusters. The heat capacities, quenched energy distributions, and Landau free energies are calculated and used to address the nature of the structural transformations that occur with increasing temperature.

Introduction

Water clusters have been the subject of numerous recent experimental and theoretical studies.[1−20] Despite the progress that has been made in delineating the properties of these fascinating species, relatively little is known about their finite temperature behavior. An exception is the water octamer for which several simulations have provided evidence of a “melting” transition.[13,14,21−25] However, the situation concerning other small water clusters is less clear. For example, there have been conflicting reports as to whether $(H_2O)_6$ undergoes a melting transition.[13,14,26−28] The presence of a pronounced peak in the heat capacity versus temperature curves is often taken as an indicator of a phase change in a cluster. However, isomerizations can also give rise to peaks in the heat capacity curve, making it necessary to use other criteria in establishing whether transformations should be viewed as phase changes or isomerizations.

Cluster systems can prove particularly challenging for computer simulations, as their potential energy surfaces often possess large numbers of minima, separated by large potential energy barriers. This can result in the trapping of the cluster in local regions of configuration space, thereby preventing the attainment of equilibrium. In this paper, the parallel-tempering Monte Carlo algorithm,[29−31] which has proven highly successful in dealing with quasiergodic behavior, is used to calculate the finite-temperature properties of the $(H_2O)_{6-9}$ clusters. Heat capacity curves, quenched energy distributions, and Landau free energies[32] are used to determine whether the clusters are undergoing melting-like transitions. Although these clusters have been considered in previous theoretical studies,[1,2,13,18,19,23−28] all four clusters have not been treated using the same theoretical approach, detailed information on the inherent structure distribution is available only for $(H_2O)_6$ and $(H_2O)_8$, and the Landau free energy has been calculated only for $(H_2O)_8$.

Computational Details

A. Potential Model. The TIP4P two-body rigid-monomer potential[33] is used to describe the water−water interaction. In this model, the water molecules interact through Coulombic and Lennard-Jones 12−6 terms. The TIP4P model has been found to give structures and relative energies of small water clusters in surprisingly good agreement with those obtained from polarizable models and from *ab initio* MP2 calculations.[13]

B. Monte Carlo Procedure. Water clusters tend to have complex potential energy surfaces, and as a result, achieving equilibrium in Monte Carlo or molecular dynamics simulations can be problematic. In this study, the parallel-tempering Monte Carlo procedure, which has proven particularly successful in achieving equilibrium in “difficult” (complex potential energy surfaces) systems,[29,35] is employed. The parallel-tempering Monte Carlo method is closely related to the jump-walk Monte Carlo method,[36] which was used in earlier studies of $(H_2O)_6$ and $(H_2O)_8$.[23,25] In the following discussion, a brief overview is first given for the jump-walk method, followed by a description of the parallel-tempering procedure.

A jump-walk Monte Carlo simulation is initiated by performing a standard Metropolis Monte Carlo simulation[34] at a temperature T_1, which is sufficiently high so that all important energy barriers are readily crossed. A subset of configurations from the initial trajectory is saved, and a second simulation is then performed at a lower temperature T_2 with most of the moves being generated by Metropolis sampling and the remainder by sampling from the configurations saved in the T_1 simulation. A subset of configurations sampled in the T_2 simulation is retained for subsequent use in a simulation at a lower temperature T_3, and the procedure is continued until the temperature range of interest is spanned. The acceptance criterion for the jump moves is

$$\mathrm{acc}(\vec{r}_{i+1} \rightarrow \vec{r}_i) = \min[1,\exp\{-(\beta_i - \beta_{i+1})(U(\vec{r}_{i+1}) - U(\vec{r}_i))\}] \quad (1)$$

where $\vec{r}_{i+1}$ refers to the current configuration in the T_{i+1} simulation and $\vec{r}_i$ is a randomly chosen configuration from the subset of configurations saved from the T_i simulation. β_i and β_{i+1} are related to the inverse temperatures $(k_bT_i)^{-1}$and $(k_bT_{i+1})^{-1}$ respectively, and $U(\vec{r}_i)$ and $U(\vec{r}_{i+1})$ are the potential energies of the configurations sampled at the two temperatures. The temperature difference between T_{i+1} and T_i must be small enough so that there is a significant overlap between the potential energy distributions of the two simulations, which, in turn, ensures that a sizable fraction of the jump moves is accepted. In the present study, the temperatures were chosen so that approximately 50% acceptance of the jump moves was achieved.

---

* Corresponding author. E-mail: jordan@imap.pitt.edu.

[†] Current address: Henry Eyring Center for Theoretical Chemistry, Department of Chemistry, University of Utah, Salt Lake City, UT 84112.

10.1021/jp030355f CCC: $25.00

TABLE 1: Details of the Parallel-tempering Monte Carlo Simulations

system	no. of production cycles[a]	jump or exchange frequency[b]	temp range[c]	constraining sphere radius (Å)
$(H_2O)_6$	2×10^8	600	15−200 K (24)	3.75
$(H_2O)_7$	2×10^8	700	40−220 K (36)	3.75
$(H_2O)_8$	2×10^8	800	70−280 K (25)	4.25
$(H_2O)_9$	2.5×10^8	900	100−290 K (44)	5.50

[a] A move includes both an attempted translation and an attempted rotation of a water monomer. 2×10^8 equilibration moves were used for each cluster. [b] Number of standard Monte Carlo moves between attempted exchanges. [c] The numbers of temperatures used are given in parentheses.

The parallel-tempering algorithm is similar to the jump-walk algorithm except that jump moves are replaced by exchange moves and that the simulations for the entire set of temperatures, $\{T_j\}$, are carried out in parallel. The acceptance criterion for an exchange between two configurations $\vec{r}_n$ and $\vec{r}_m$ generated in simulations at the respective temperatures T_n and T_m is

$$\mathrm{acc}(\vec{r}_n \rightarrow \vec{r}_m) = \min[1, \exp\{-(\beta_m - \beta_n)(U(\vec{r}_n) - U(\vec{r}_m))\}] \tag{2}$$

A major advantage of this method is that the storage of configurations is unnecessary, because the exchange configurations are generated "on the fly". Thus, for long simulations, the number of configurations available for an exchange is much larger than would be available in a jump-walk simulation, which can greatly improve convergence to equilibrium. In addition, the correlations between the configurations generated at different temperatures are generally less in parallel-tempering than in jump-walk simulations.[29] As for the jump-walk procedure, the highest temperature should permit the barriers to be surmounted, and there must be appreciable overlap between the potential energy distributions from the simulations (replicas) at adjacent temperatures.

An additional requirement for successful finite temperature simulations of cluster systems is the exclusion of evaporative events, which can propagate downward in temperature in jump-walk and parallel-tempering simulations and introduce errors in the low temperature results. In this study, a constraining sphere is used to prevent evaporation. For each trial move, the cluster's center of mass is located at the origin of the constraining sphere. If any molecule is located outside the constraining sphere, the trial move is rejected. The constraining sphere radius must be small enough to prevent evaporation, yet large enough so that the cluster geometries are not appreciably distorted. For large clusters, it is sometimes not possible to satisfy both these requirements, making it preferable to adopt alternative strategies for excluding evaporative events. However, this was not a problem for the size clusters considered here. The constraining sphere radii were ranged from 3.75 Å for $(H_2O)_6$ to 5.50 Å for $(H_2O)_9$.

In the present work, parallel-tempering Monte Carlo simulations were performed on each of the $(H_2O)_{6-9}$ clusters. In these studies, exchanges were attempted only between configurations for simulations (replicas) at adjacent temperatures. The details of the simulations (i.e., the number of production and equilibration moves, exchange frequencies, range of temperatures employed, and constraining sphere radii) are given in Table 1. At each temperature in the parallel-tempering simulations, 2.0 × 10^8 production moves were employed for $(H_2O)_6$, $(H_2O)_7$, and $(H_2O)_8$, whereas 2.5 × 10^8 production moves were employed for $(H_2O)_9$. The production moves were preceded by 2 × 10^8 equilibration moves for each of the clusters. The temperature ranges considered were 15−200, 40−220, 70−280, and 100−290 K for $(H_2O)_6$, $(H_2O)_7$, $(H_2O)_8$, and $(H_2O)_9$, respectively. The simulations employed from 25 to 44 temperatures. For the standard Metropolis steps, translational and rotational moves were attempted in succession for molecules selected at random. On the basis of comparison of the results obtained from shorter simulations and on the insensitivity of the results to the choice of the initial configuration, we are confident that the simulations have achieved equilibration.

C. Melting criteria. A commonly used criterion for a phase change is the appearance of a pronounced peak in the heat capacity versus temperature curve.[37] In this study, the heat capacity is calculated from the potential energy fluctuations

$$C_{\mathrm{N,V,T}} = \frac{\langle U^2 \rangle - \langle U \rangle^2}{RT^2} + \frac{M}{2} R \tag{3}$$

where R is the gas constant and M is the number of degrees of freedom.

For a transition to be properly described as melting, it is essential that there be a sufficiently high density of states in the high temperature "phase". In clear-cut cases, this manifests itself in a bimodal potential energy distribution or a double minimum in the free energy as a function of an order parameter. In this work, Landau free energy curves[32] are calculated as a function of two different order parameters. In addition, the inherent structures[38] are obtained by quenching configurations generated at different temperatures. The following subsections describe the Landau free energy calculations and the quenching methodology.

D. Landau Free Energy Curves. The calculation of the Landau free energy as a function of an order parameter is based upon an approach pioneered by Lynden-Bell and Wales who proposed that "if an order parameter, χ, can be found such that the Landau free energy has double minima as a function of χ, then two distinct phases can be said to coexist".[32] The existence of the double minimum in the free energy curve indicates that a free energy barrier exists between two distinct phases. In using the Landau free energy, it is necessary to identify an order parameter that is a smooth function of the $3N$ atomic coordinates and is invariant with respect to translations and rotations of the cluster's coordinate frame. In this study Q_4,[32] which is based on bond orientations, and U, the potential energy, are employed as order parameters. In general, qualitatively similar results are obtained for the two order parameters, and only those based on the potential energy are reported here.

E. Quenching Methodology. Quenching of configurations sampled in a simulation allows one to determine the populations of various inherent structures.[38] In this study, subsets of the configurations generated at various temperatures were quenched (optimized) using the "Orient" program,[39] and the resulting structures were binned according to the energy. In those cases in which different isomers are very close in energy, different structures can end up in the same bin. This problem was avoided by visually inspecting the quenched structures. The quenched distribution plots, when combined with the Landau free energy curves, provide insight into the structural changes associated with the peaks in the heat capacity curves.

Results

The heat capacity versus T curves for $(H_2O)_{6-9}$ as described by parallel-tempering simulations are shown in Figure 1. For $(H_2O)_6$ and $(H_2O)_8$, the resulting heat capacity curves are in

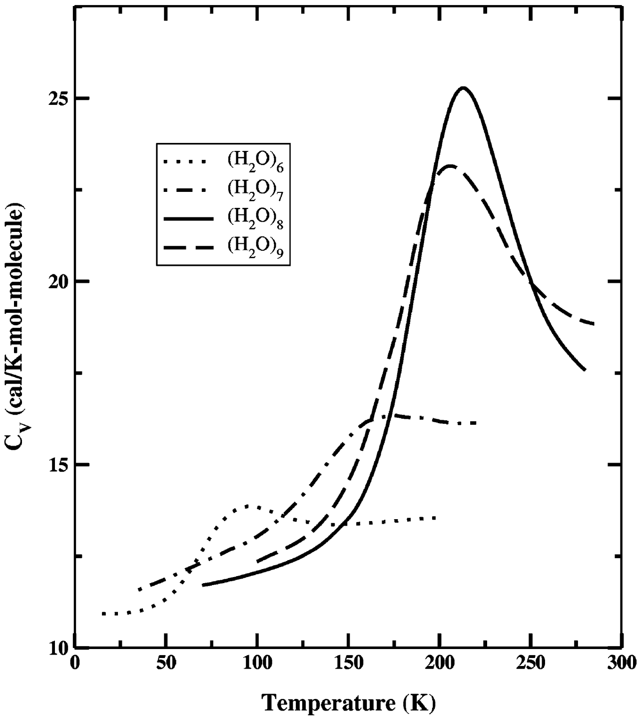

Figure 1. Heat capacity curves of $(H_2O)_{6-9}$ calculated by means of parallel-tempering Monte Carlo simulations.

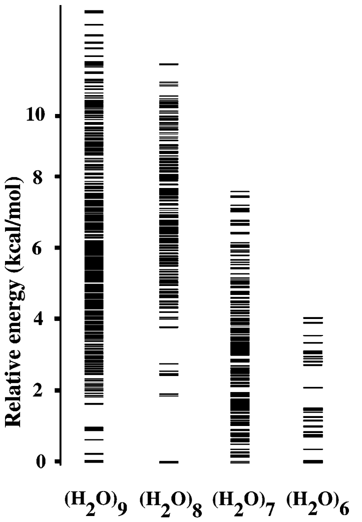

Figure 2. Relative energies of the potential energy minima of $(H_2O)_{6-9}$ determined by quenching configurations sampled in the parallel-tempering Monte Carlo simulations.

close agreement with those obtained from prior jump-walk and parallel-tempering simulations.[18,23,25,40] The heat capacity curves of $(H_2O)_8$ and $(H_2O)_9$ have pronounced peaks near 212 and 207 K, respectively. In contrast, the heat capacity curves of $(H_2O)_6$ and $(H_2O)_7$ display only very weak peaks (near 90 and 170 K, respectively). In analyzing these results, it is useful to refer to the distributions of local potential energy minima depicted in Figure 2. $(H_2O)_8$ has the smallest number of low-energy minima (here, low energy is arbitrarily taken to mean $\leq$ 2 kcal/mol). Specifically, it has two nearly isoenergetic low-lying cubic-like minima (of S_4 and D_{2d} symmetry) followed by an energy gap of 1.8 kcal/mol from a group of six higher-lying cubic-like structures, with a high density of noncubic structures starting at about 3.8 kcal/mol. $(H_2O)_9$ has nine local minima between 0 and 1.8 kcal/mol, with a high density of local minima starting near 2.0 kcal/mol. $(H_2O)_6$, although having a comparable number of low-energy minima as $(H_2O)_9$ does not display a high density of local minima at energies more than 2.0 kcal/mol above the global minimum). $(H_2O)_7$, on the other hand, has a high density of local minima, starting just above the global minimum in energy. In presenting the detailed results for the individual clusters, $(H_2O)_8$ and $(H_2O)_9$ are considered first because they show the most pronounced structure in the heat capacity curves.

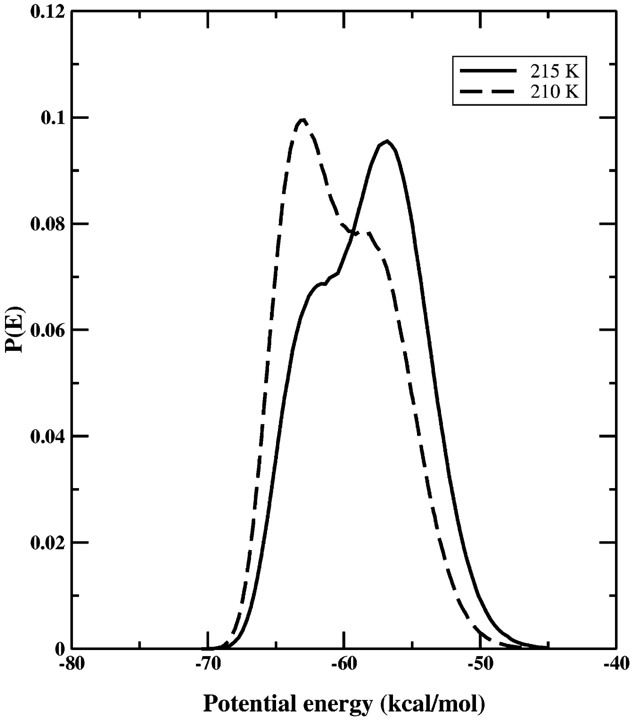

Figure 3. Histograms of potential energies of $(H_2O)_8$ from the T = 210 and 215 K replicas from a parallel tempering Monte Carlo simulation.

A. $(H_2O)_8$ Results. Figure 3 shows the potential energy histograms for the T = 210 and 215 K replicas from the parallel tempering simulations on $(H_2O)_8$. These temperatures bracket that associated with the peak of the heat capacity curve. The histograms are bimodal, consistent with the interpretation of coexisting phases.[18,23,25]

Figure 4 depicts the structures of the 20 lowest-energy minima (shown in order of increasing energy) of $(H_2O)_8$ obtained by quenching configurations saved at each temperature in the parallel-tempering simulations. As noted above, $(H_2O)_8$ has two low-energy cubic structures (of S_4 and D_{2d} symmetry) followed by a sizable (~2 kcal/mol) energy gap, then six more cubic-like structures.[25] At still higher energies, there are other cubic structures plus a large number of non-cubic structures. Figure 5 shows the population distributions of different inherent structures as a function of temperature. At temperatures below 160 K, the two low-energy cubic $(H_2O)_8$ configurations dominate the population distributions. As the temperature increases beyond 160 K, the populations of these two cubic structures rapidly decrease and the populations of the noncubic species rapidly grow. The higher energy cubic structures are most important around 215 K but never account for more than 12% of the total population. It is clear from this figure that the pronounced peak in the heat capacity curve is due to a transition from the two low-energy cubic structures to the higher-energy noncubic structures rather than to the higher-energy cubic structures. This is consistent with the conclusions of Nigra et al.[18]

Figure 6 reports for $(H_2O)_8$ the Landau free energy as a function of the potential energy. The Landau free energy curves

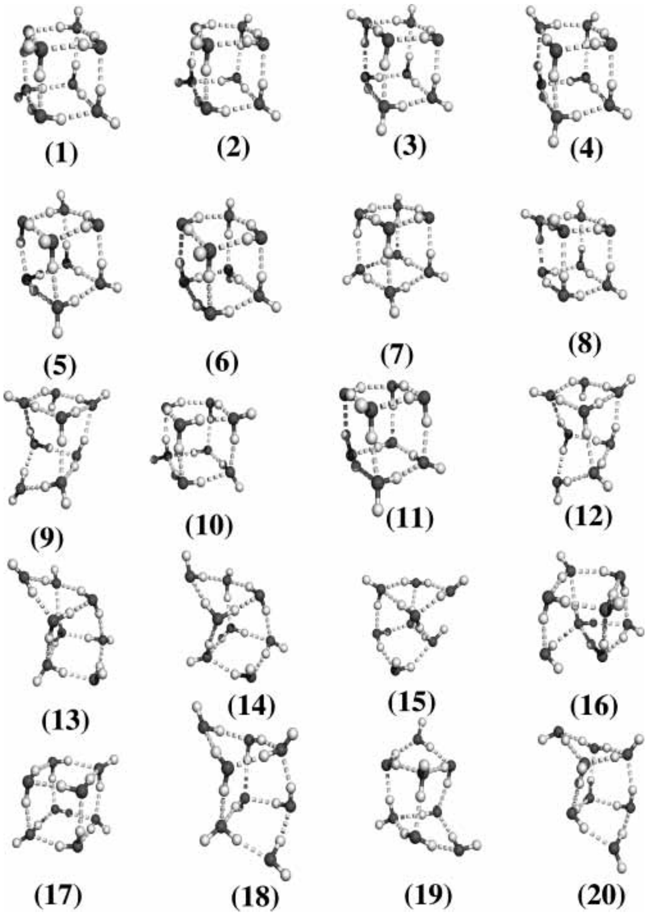

Figure 4. Structures of the 20 lowest-energy minima of $(H_2O)_8$ found in the parallel-tempering simulations.

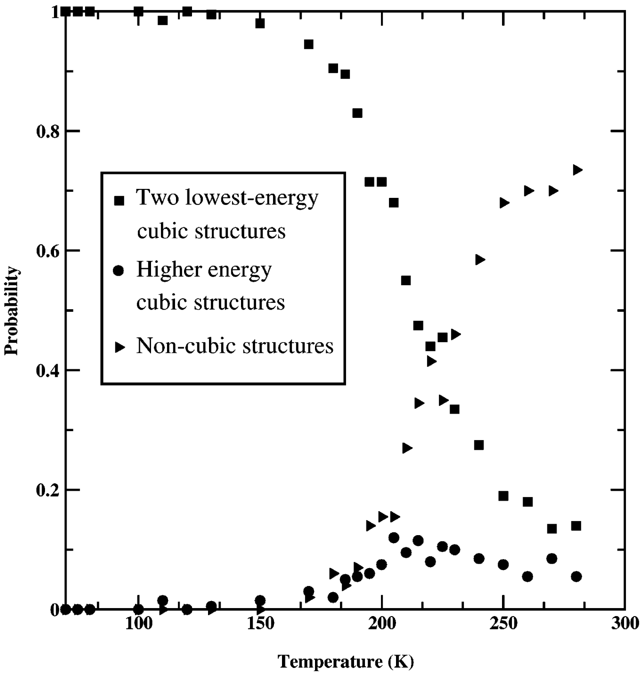

Figure 5. Distributions of various inherent structures of $(H_2O)_8$ as a function of temperature. Results from parallel-tempering simulations.

display a minimum with a shoulder at either high or low energy, consistent with the coexistence of two phases. The Landau free energy curves associated with the 210 and 215 K replicas have very flat minima, consistent with the presence of two phases of nearly the same free energy.

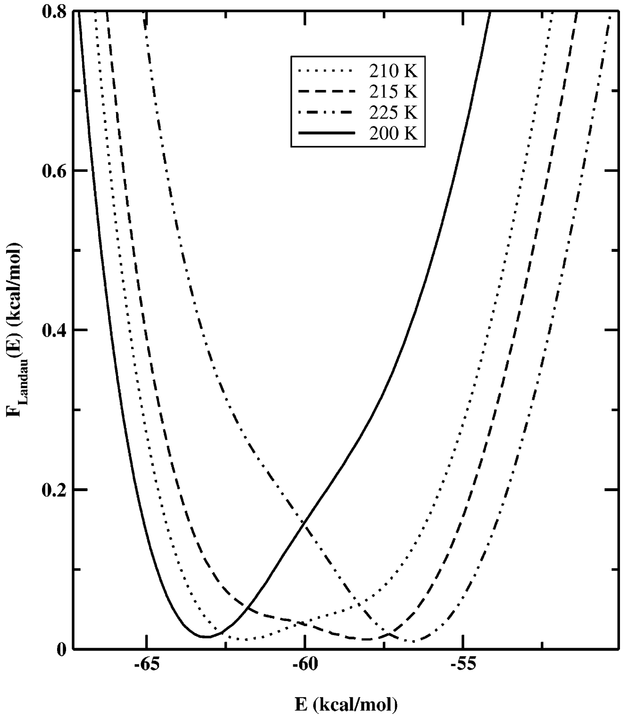

Figure 6. Landau free energies for $(H_2O)_8$ calculated as a function of the potential energy. Results are based on parallel-tempering Monte Carlo simulations.

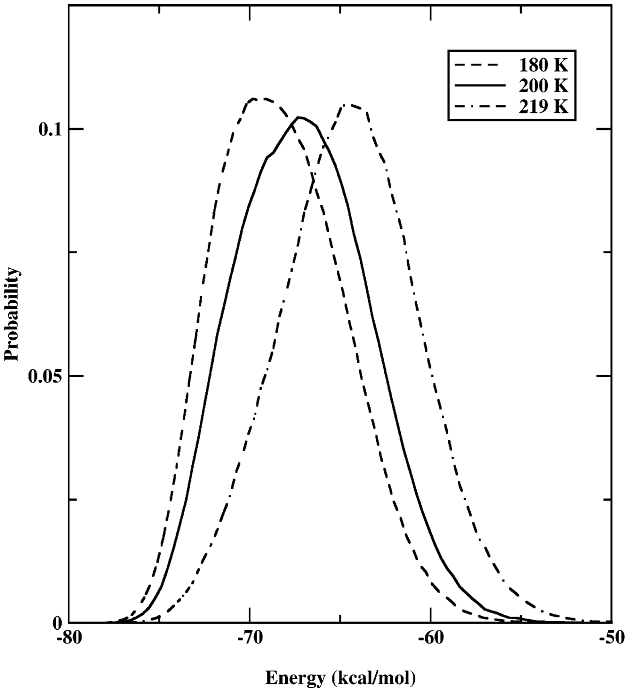

Figure 7. Histograms of potential energies of $(H_2O)_9$ from the T = 180, 200, and 219 K replicas from a parallel tempering Monte Carlo simulation.

B. $(H_2O)_9$ Results. The heat capacity curve of $(H_2O)_9$ is qualitatively similar to that of $(H_2O)_8$. The peak of the heat capacity curve of $(H_2O)_9$ occurs near 207 K and has an approximate value of 23 cal/K-mol-molecule. The potential energy distributions of $(H_2O)_9$ obtained from parallel-tempering simulations carried out at 180, 200, and 219 K, are shown in Figure 7. In contrast to $(H_2O)_8$, for $(H_2O)_9$, the potential energy distributions from replicas at temperatures close to that of the peak in the heat capacity curve do not show bimodality.

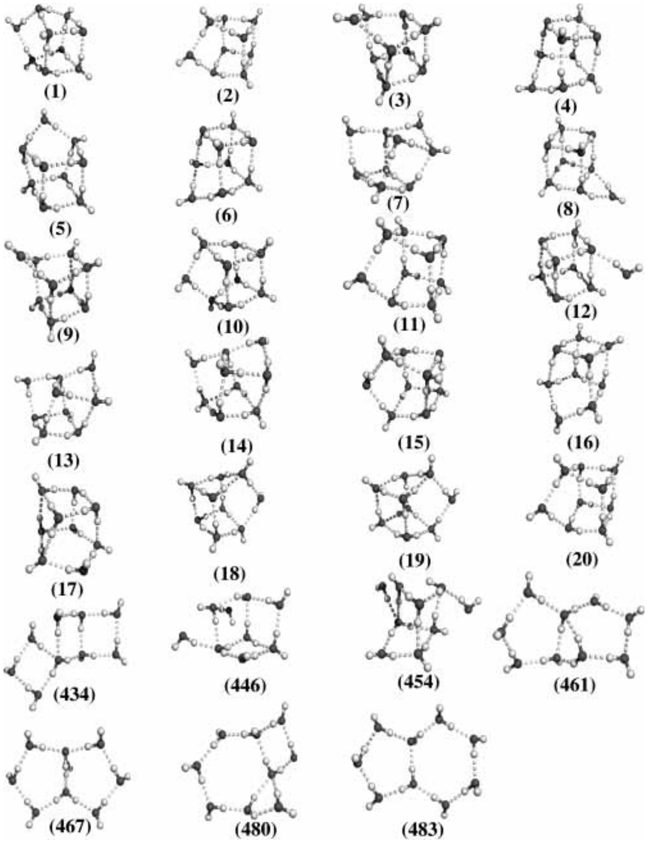

Figure 8. Structures of the 20 lowest-energy minima and seven representative high-energy minima of $(H_2O)_9$ found in parallel-tempering Monte Carlo simulations.

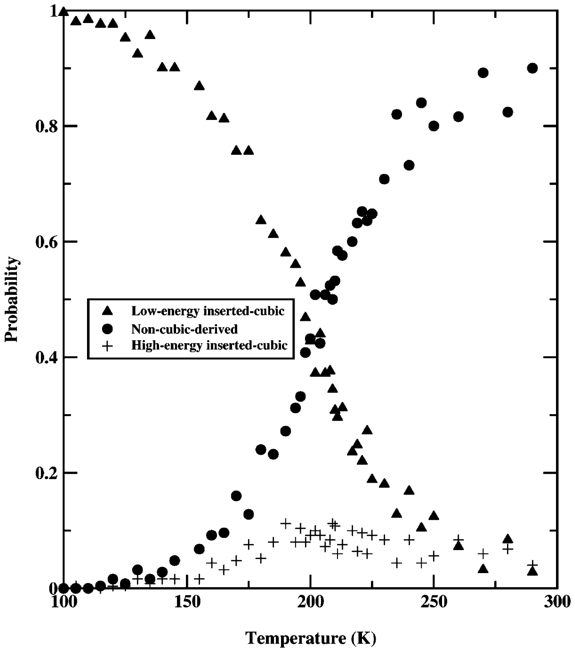

Figure 9. Distributions of various inherent structures of $(H_2O)_9$ as a function of temperature. Results obtained from the parallel-tempering Monte Carlo simulations.

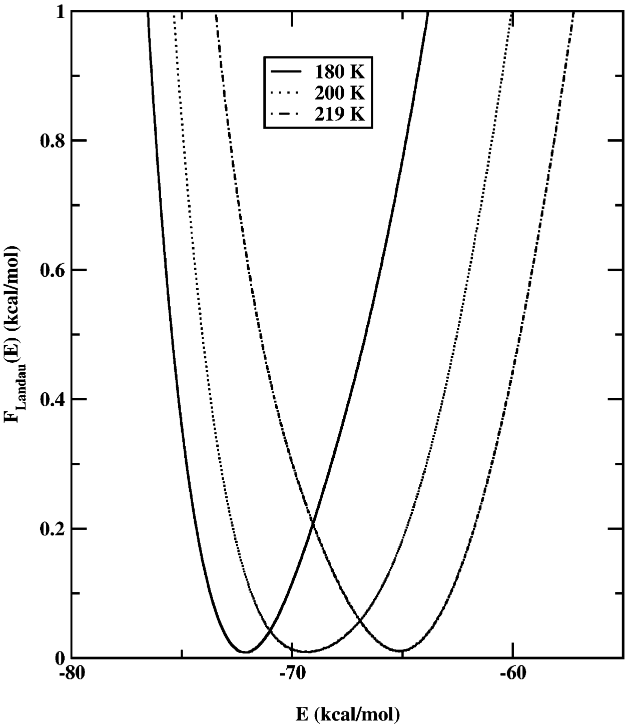

Figure 10. Landau free energy curves of $(H_2O)_9$ calculated as a function of the potential energy. Results are reported for parallel tempering Monte Carlo simulations carried out at $T = 180$, 200, and 219 K.

However, the widths of these distributions are only slightly narrower than those of $(H_2O)_8$ calculated at temperatures close to the maximum in its heat capacity curve. This strongly suggests that the potential energy distributions of $(H_2O)_9$ arise from two overlapping distributions.

Figure 8 depicts the structures, in order of increasing energy, of the 20 lowest-energy minima of $(H_2O)_9$ found in the quenching calculations. The low-energy structures can be viewed as resulting from inserting a water molecule into one of the edges of one of the two low-energy cubic forms of $(H_2O)_8$.[9] We refer to these as "inserted-cubic" species. There are additional, higher-energy inserted-cubic structures that can be viewed as resulting from insertion of a water molecule into the edge of one of the higher-energy cubic structures of $(H_2O)_8$. Finally, there is a very large number of other structures, a few of which are shown in Figure 8.

Figure 9 reports the distributions of various inherent structures as a function of temperature. The structures are divided into three classes: low-energy inserted-cubic (species 1−4, 6, and 8 in Figure 8), higher-energy inserted-cubic structures, and non-cubic-derived isomers. At low temperatures, the quenched distributions are dominated by the low-energy inserted-cubic structures, whereas at temperatures above the peak in the heat capacity curve, the non-cubic-derived structures dominate. The higher-energy inserted-cubic structures never acquire a population above 0.12. This is analogous to the situation for $(H_2O)_8$, for which the high-energy cubic structures do not attain a high population at any temperature.

Figure 10 reports the Landau free energy of $(H_2O)_9$ calculated at each of $T = 180$, 200, and 219 K and using the potential energy as the order parameter. None of the Landau free energy curves displays double minima, although that calculated using configurations sampled in the $T = 200$ K replica does show slight broadening at low free energies. The Landau free energy curves calculated using the Q_4 order parameter (not shown) also did not show double minima in this case. We note, however, that it may be possible to devise an order parameter that would display such behavior.

To gain additional insight into the lack of bimodality in the potential energy distributions and the lack of a double-well

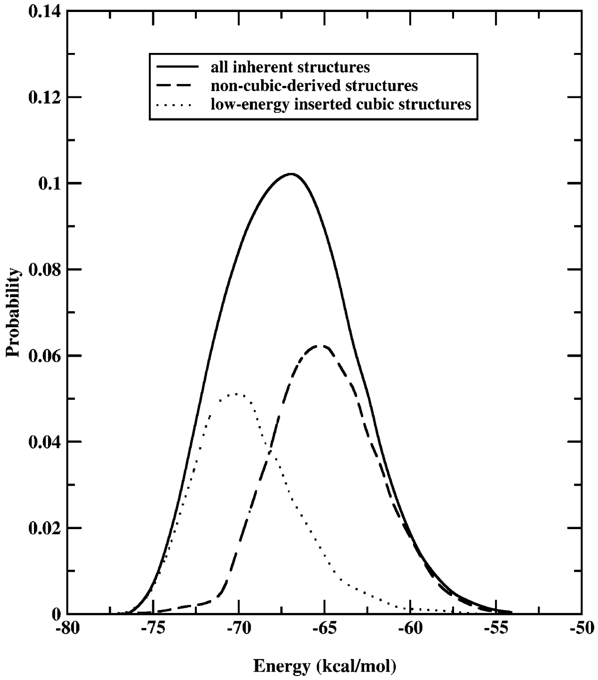

Figure 11. Potential energy distributions of configurations of $(H_2O)_9$ sampled in the 200 K replica from the parallel-tempering Monte Carlo simulations. The two classes of sampled structures (low-energy inserted-cubic and non-cubic-derived) are identified according to the inherent structures to which they quench.

character in the Landau free energy curves of $(H_2O)_9$, each configuration sampled in the $T = 200$ K replica was quenched to its inherent structure. The quenched configurations were divided into two groups, the low energy inserted-cubic structures and the non-cubic-derived structures. In Figure 11 we plot the potential energy distribution of the configurations that quench to each of these two groups. It is clear from this representation of the data that the single peak in the potential energy distribution from the $T = 200$ K simulation (Figure 7) derives from two overlapping distributions (i.e., from inserted-cubic and non-cubic-derived clusters).

For comparative purposes, we have carried out a similar analysis on the configurations from the $T = 215$ K replica from the parallel-tempering simulation on $(H_2O)_8$. Figure 12 plots the potential energy distribution of the configurations that quench to the two lowest-energy cubic structures and those that quench to noncubic structures. Comparison of the distributions reported in Figures 4 and 12 reveals that the bimodal nature of the distributions in Figure 4 arises from the overlap of two distributions, one due to cubic-type structures and the other to noncubic structures. In the case of $(H_2O)_8$, the peaks from the two distributions are separated by about 12 kcal/mol, whereas in the case of $(H_2O)_9$ they are separated by only 6 kcal/mol. This is consistent with the smaller energy gap between the inserted cubic and non-cubic-derived isomers of $(H_2O)_9$ than between the cubic and non-cubic isomers of $(H_2O)_8$.

C. $(H_2O)_6$ Results. Potential energy histograms for the $T = 15$, 45, 65, 70, 100, and 135 K replicas from the parallel tempering simulations on $(H_2O)_6$ are shown in Figure 13. There is no evidence of bimodality in any of the potential energy histograms; nor does there appear to be broadening of the distribution obtained from the replica at $T = 100$ K, which is close to the temperature of the maximum in the broad peak in the heat capacity curve).

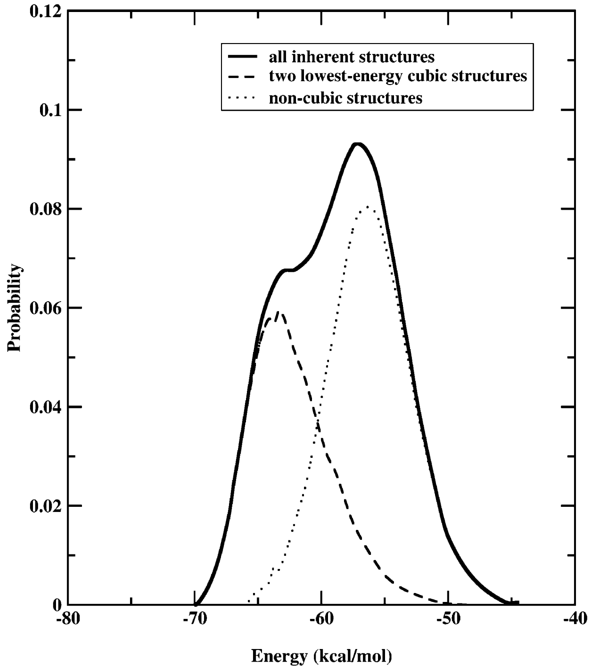

Figure 12. Potential energy distributions of configurations of $(H_2O)_8$ sampled in the 215 K replica from the parallel-tempering Monte Carlo simulations. The two classes of sampled structures (two lowest-energy cubic and noncubic) are identified according to the inherent structures to which they quench.

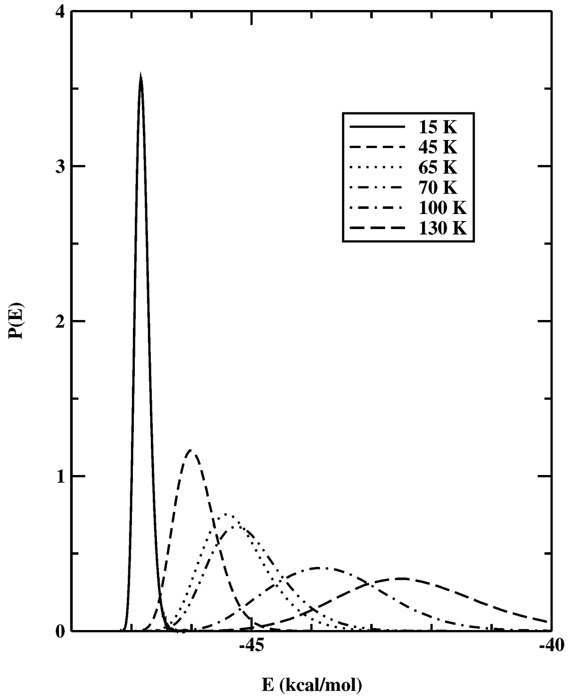

Figure 13. The potential energy histograms of $(H_2O)_6$ obtained from the 15, 45, 65, 70, 100, and 130 K replicas from a parallel-tempering Monte Carlo simulation.

Figure 14 depicts the low-lying inherent structures found by quenching configurations generated in the parallel-tempering simulations on $(H_2O)_6$. As has been previously reported, with the TIP4P potential, $(H_2O)_6$ has two low-lying cage-like minima, followed at somewhat higher energy by five prism structures.[25] Even at energies as high as 4 kcal/mol above the global minimum, the density of local minima is quite sparse when compared to the densities of local minima of the $(H_2O)_7$ and $(H_2O)_9$ clusters.

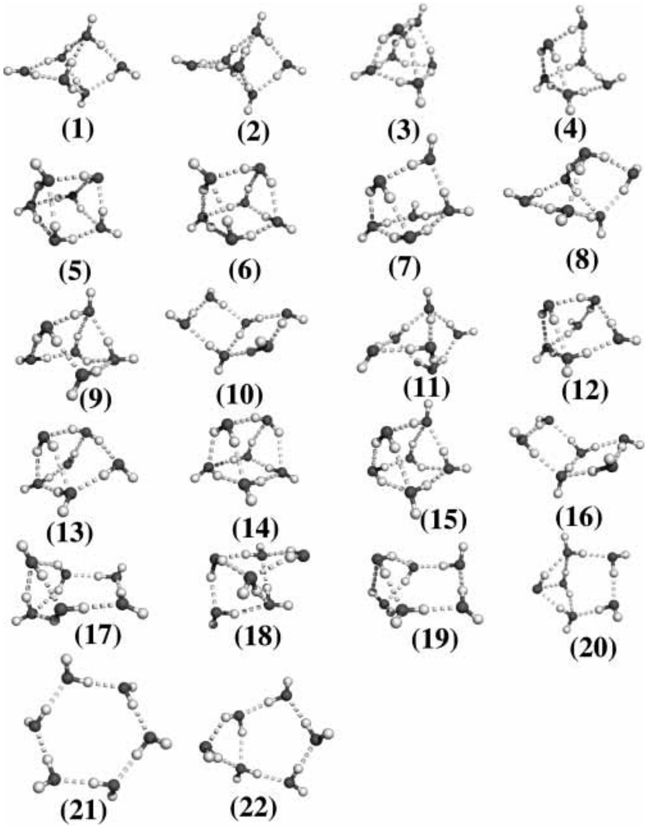

Figure 14. Structures of the 22 lowest-energy minima of $(H_2O)_6$ found by quenching configurations from the parallel-tempering Monte Carlo simulations.

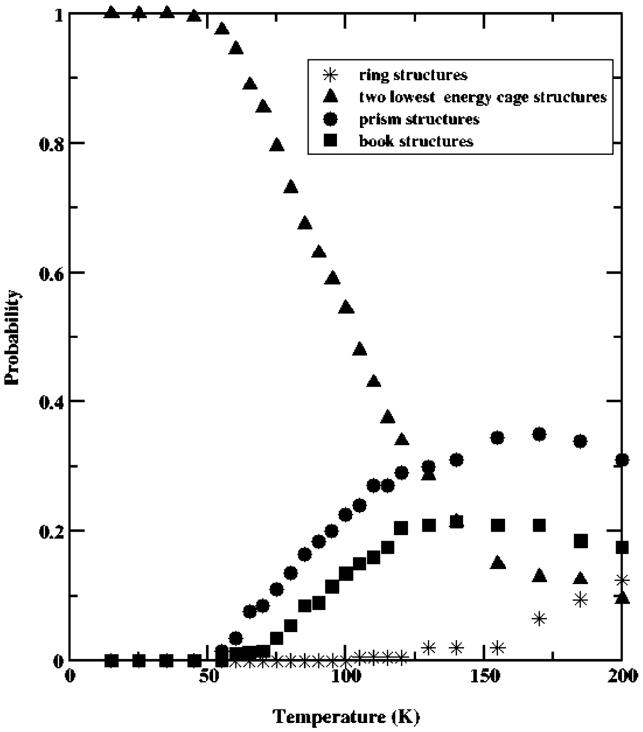

Figure 15. Distributions of the inherent structures of $(H_2O)_6$ as a function of temperature. Results are from parallel-tempering Monte Carlo simulations.

The distributions of the inherent structures from the quench calculations are shown in Figure 15. At temperatures below 50 K, the two low-lying cage configurations dominate the distributions. As the temperature is increased above 50 K, the population of these cage structures decreases, and the populations of prism and book structures grow in importance, with the latter having their maxima near $T = 160$ and 135 K, respectively. The ring-type structures have a small (<2%) population for $T = 130-155$ K and grow in importance as T is increased above 155 K.

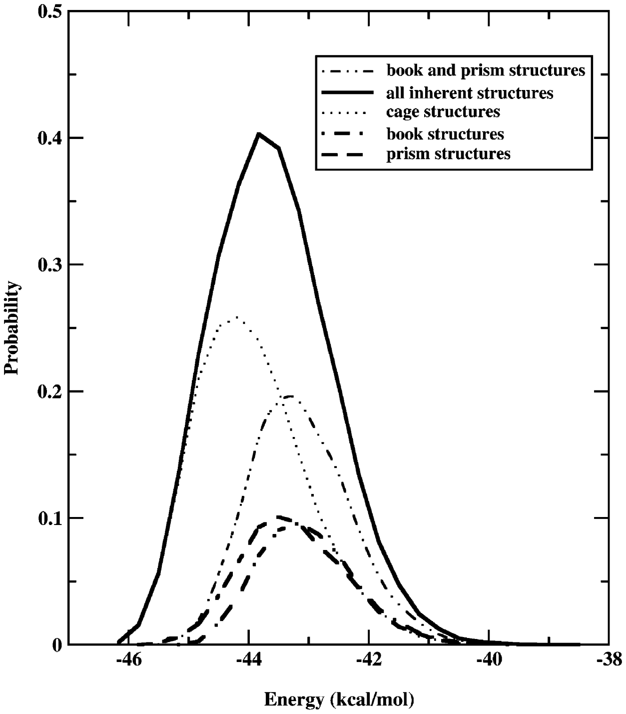

Figure 16. Potential energy of configurations of $(H_2O)_6$ sampled in the 100 K replica from the parallel-tempering Monte Carlo simulations. The different classes of sampled structures (cage, book, and prism) are identified according to the inherent structures to which they quench.

Each configuration sampled in the 100 K replica was quenched to its inherent structure, and the distributions of configurations that quench to the cage structures, prism, and book structures are separately plotted in Figure 16. These three distributions are appreciably overlapped, with their peaks being separated by less than 1 kcal/mol. The Landau free energy curves for $(H_2O)_6$ derived from the 25, 45, 80, and 100 K replicas and using the potential energy as the order parameter are shown in Figure 17. None of the Landau free energy curves displays bimodal character.

D. $(H_2O)_7$ Results. The heat capacity curve of $(H_2O)_7$, depicted in Figure 1, has a very broad, weak peak centered near 175 K. The potential energy histograms of the configurations, shown in Figure 18, do not display bimodality.

Figure 19 depicts a subset of the low energy inherent structures of $(H_2O)_7$. These are grouped into three categories. Minima 1, 2, 4, and 6, which can be viewed as being derived from a cubic $(H_2O)_8$ cluster by extraction of a water molecule, are grouped into category I; minima 3, 5, 8, and 18, which can be viewed as being formed by adding a water monomer to a cage form of the hexamer, are grouped together in category II; all other structures are placed in Category III.

The distributions of the inherent structures in the different categories are shown in Figure 20. At temperatures below about 150 K, category I structures dominate the population. Starting near 100 K, the category II structures rapidly increase in importance. At 175 K, near the temperature corresponding to the peak of the $(H_2O)_7$ heat capacity curve, category I, II, and

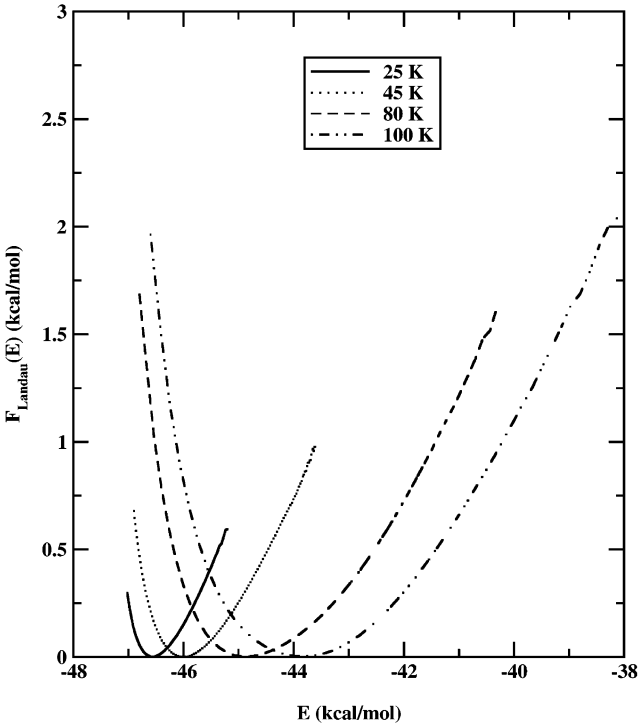

Figure 17. Landau free energies for $(H_2O)_6$ calculated as a function of the potential energy. Results are based on parallel-tempering Monte Carlo simulations.

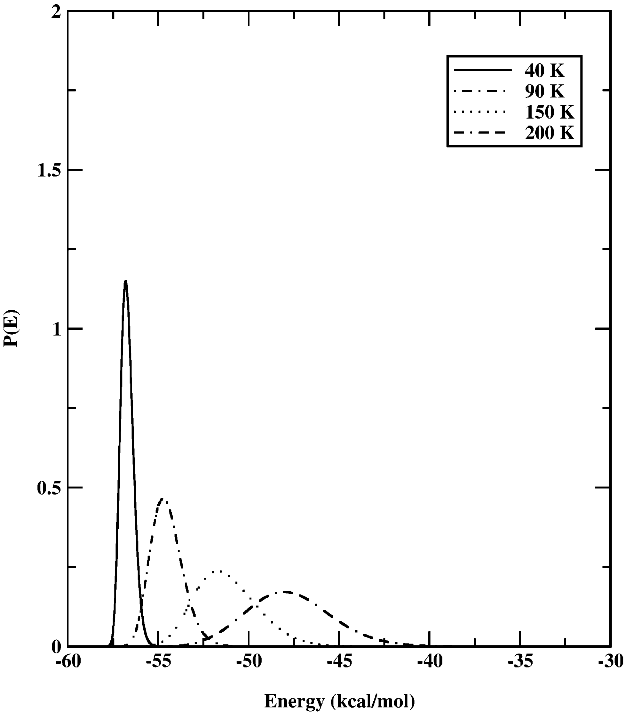

Figure 18. Histograms of potential energies of $(H_2O)_7$ obtained from parallel-tempering Monte Carlo simulations.

III structures comprise approximately 62, 30, and 8% of the population, respectively.

The configurations sampled in the 175 K replica were quenched to their inherent structures and used to generate Figure 21, which reports the distributions of the sampled configurations that quench to inherent structures in each of the three categories discussed above. The distributions associated with inherent structures belonging to categories II and III fall under the distribution associated with category I, with the peaks in the three distributions falling within 1 kcal/mol of one another.

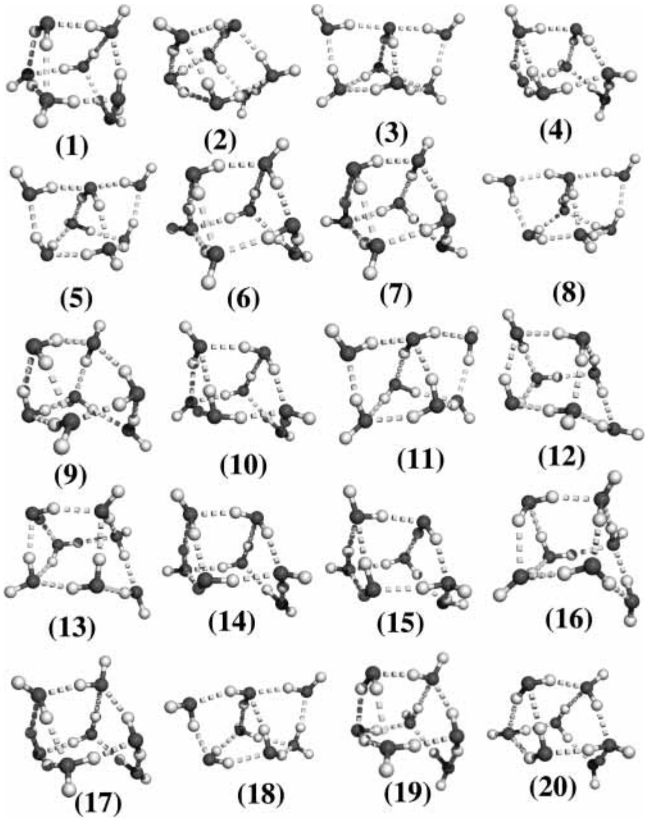

Figure 19. Structures of the 20 lowest-energy minima of $(H_2O)_7$ from the parallel-tempering Monte Carlo simulations.

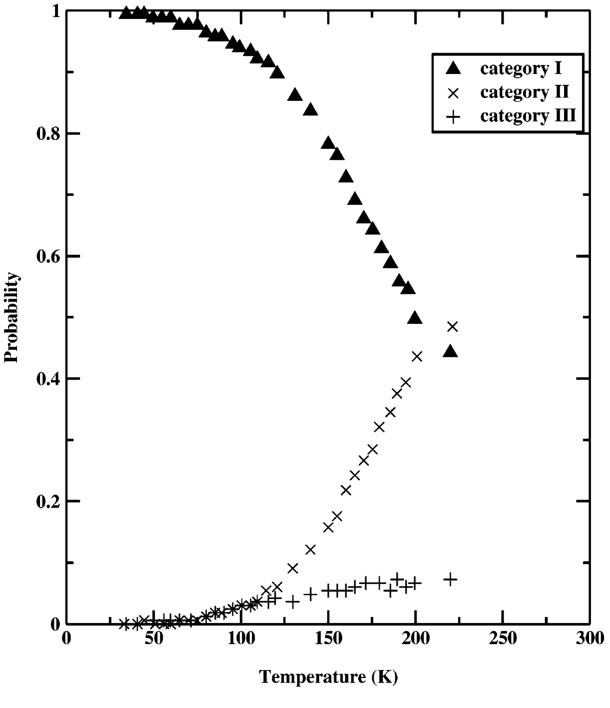

Figure 20. Distributions of the inherent structures of $(H_2O)_7$ as a function of temperature. Results are based on parallel-tempering Monte Carlo simulations.

The dependence of the Landau free energy of $(H_2O)_7$ on the potential energy order parameter is depicted in Figure 22. Results are reported for the $T = 40$, 90, 150, and 200K replicas. None of the free energy curves display double minima character.

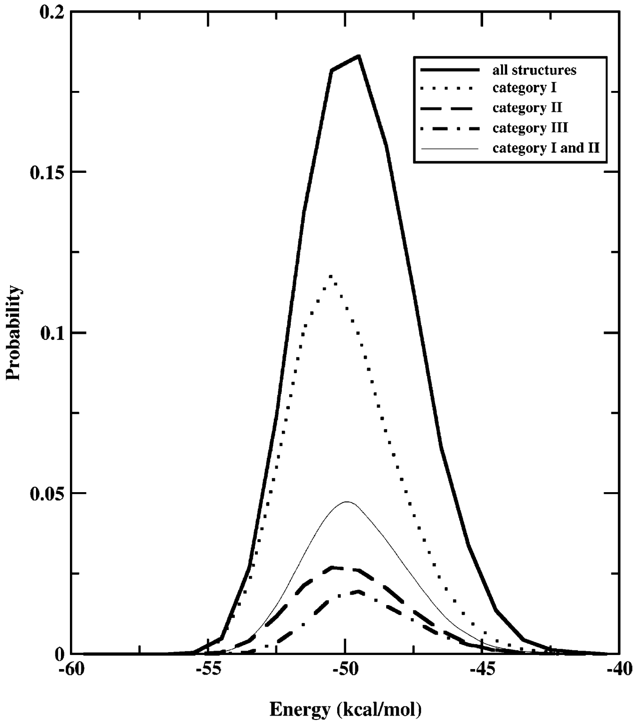

Figure 21. Distributions of configurations of $(H_2O)_7$ that quench to inherent structures belonging to categories I, II, and III. Results from the parallel-tempering Monte Carlo simulation carried out at 175 K.

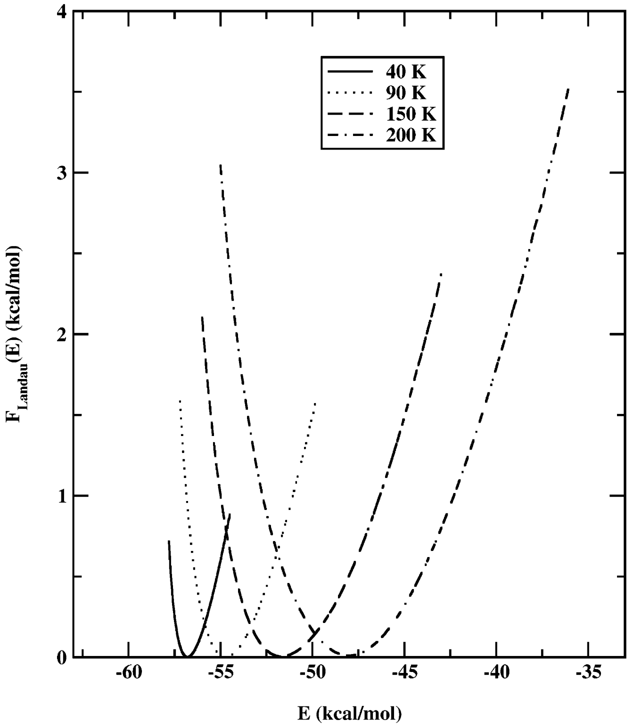

Figure 22. Landau free energy curves for $(H_2O)_7$ calculated as a function of the potential energy. Results are based on parallel-tempering Monte Carlo simulations.

Discussion and Conclusions

The heat capacity curves of $(H_2O)_8$ and $(H_2O)_9$ display pronounced peaks near 212 and 205 K, respectively, while those for $(H_2O)_6$ and $(H_2O)_7$ display much weaker, broader peaks at lower temperatures. In the case of $(H_2O)_8$, the peak in the heat capacity is due to the transition from the two low-energy cubic structures to the noncubic structures. For $(H_2O)_9$, the peak in the heat capacity curve derives from the analogous transition between low-energy inserted-cubic structures to non-cubic-derived structures. The peak in the heat capacity curve of $(H_2O)_6$ is due to a transition from the low-energy, cage-like structures to prism and book-like structures, and that in the heat capacity of $(H_2O)_7$ is due to a transition from category I to category II plus III structures. This can be viewed as a transformation between depleted-cubic structures (cubic structures missing one water molecule) to type II and III structures.

We now address the issue of whether these structural transformations should be viewed as melting transitions. Only in the case of $(H_2O)_8$ does the potential energy distribution display bimodal character and does the plot of the Landau free energy versus potential energy order parameter show clear-cut phase coexistence. We conclude, therefore, that the transformation occurring near 212 K in $(H_2O)_8$ is a melting transition.

The failure of the potential energy histograms and Landau free energy curves of $(H_2O)_9$ to display behavior characteristic of phase coexistence is somewhat surprising, given the pronounced peak in the heat capacity versus T curve of this cluster. However, by associating the sampled configurations with the inherent structures to which they quench, it is demonstrated that the single peak in the potential energy histogram obtained from the $T = 200$ K replica results from two partially overlapping distributions, the peaks of which are separated by about 6 kcal/mol. A similar analysis of $(H_2O)_8$ reveals that the two distributions (cubic and noncubic) are separated by a larger amount ($\approx$12 kcal/mol) than in the $(H_2O)_9$ case, which is why clear-cut bimodal behavior is seen in the potential energy distribution of $(H_2O)_8$. Because of the relationship between the potential energy distributions and the Landau free energy curves, this also explains why the Landau free energy curves (using the potential energy as the order parameter) failed to display a double minimum for $(H_2O)_9$. If the Landau free energy were reanalyzed in terms of inherent structures, the double minima nature would become apparent. We conclude, therefore, that the transition associated with the pronounced peak in the heat capacity curve of $(H_2O)_9$ should also be viewed as arising from a melting transition.

For $(H_2O)_6$ and $(H_2O)_7$, the potential energy distributions involved in the structural transitions are strongly overlapped with peak separations of less than 1 kcal/mol. This explains why, for these clusters, the potential energy distributions fail to show bimodality, the Landau free energy curves do not display double minima, and the resulting peaks in the heat capacity curves are so weak. This different behavior of $(H_2O)_6$ and $(H_2O)_7$ from that of $(H_2O)_8$ and $(H_2O)_9$ is related to differences in the distributions of local potential energy minima of these clusters. Given the relatively low density of local minima and the trends in the quench distributions, we conclude that the weak peak in the calculated heat capacity curve of $(H_2O)_6$ should be viewed as due to a cage to (prism, book) type isomerization rather than as arising from a melting transition. We conclude also that $(H_2O)_7$, does not undergo a well-defined melting transition. However given the relatively high density of low-energy local minima of this cluster, it is possible that this cluster displays “glasslike” behavior. To establish this would require examination of the dynamics of the cluster.

Acknowledgment. This research was supported with a grant from the National Science Foundation. The calculations were carried out on a Pentium cluster at the Pittsburgh Supercomputing Center and on the IBM RS6000 workstation cluster in the University of Pittsburgh’s Center for Molecular and Materials Simulations (CMMS). The computers in CMMS were funded by grants from the National Science Foundation and IBM. We thank Professor Dave Freeman for valuable discussions about the parallel tempering algorithm.

References and Notes

(1) Wales, D. J.; Ohmine, I. *J. Chem. Phys.* **1993**, *98*, 7257.

(2) Wales, D. J.; Ohmine, I. *J. Chem. Phys.* **1993**, *98*, 7245.

(3) Wales, D. J.; Hodges, M. P. *Chem. Phys. Lett.* **1998**, *286*, 65.

(4) Jongseob, K.; Majumdar, D.; Lee, H. M.; Kim, K. S. *J. Chem. Phys.* **1999**, *110*, 9128.

(5) Lee, H. M.; Suh, S. B.; Lee, Y. L.; Tarakeshwar, P.; Kim, K. S. *J. Chem. Phys.* **2000**, *112*, 9759.

(6) Brown, M. G.; Keutsch, F. N.; Saykally, R. J. *J. Chem. Phys.* **1998**, *109*, 9645.

(7) . Liu, K.; Brown, M. G.; Carter, C.; Saykally, R. J.; Gregory, J. K.; Clary, D. C. *Nature* **1996**, *381*, 501.

(8) Liu, K.; Cruzan, J. D.; Saykally, R. J. *Science* **1996**, *271*, 929.

(9) Gruenloh, C. J.; Carney, J. R.; Hagemeister, F. C.; Zwier, T. S.; Wood, J. T.; Jordan, K. D. *J. Chem. Phys.* **2000**, *113*, 2290.

(10) Gruenloh, C. J.; Carney, J. R.; Arrington, C. A.; Zwier, T. S.; Fredericks, S. Y.; Jordan, K. D. *Science* **1997**, *276*, 1678.

(11) Gruenloh, C. J.; Carney, J. R.; Hagemeister, F. C.; Arrington, C. A.; Zweir, T. S.; Fredericks, S. Y.; Wood, J. T., III; Jordan, K. D. *J. Chem. Phys.* **1998**, *109*, 6601.

(12) Dang, L. X. *J. Chem. Phys.* **1999**, *110*, 1526.

(13) Pedulla, J. M.; Kim, K.; Jordan, K. D. *Chem. Phys. Lett.* **1998**, *291*, 78.

(14) Drozdov, S. V.; Vostrikov, A. A. *Technical Phys. Lett.* **2000**, *26*, 397.

(15) Burnham, C.; Li, J.; Xantheas, S. S.; Leslie, M. *J. Chem. Phys.* **1999**, *110*, 4566.

(16) Batista, E. R.; Xantheas, S. S.; Jonsson, H. *J. Chem. Phys.* **1999**, *111*, 6011.

(17) Stern, H. A.; Rittner, F.; Berne, B. J.; Friesner, R. A. *J. Chem. Phys.* **2001**, *115*, 2237.

(18) Nigra, P.; Carignano, M. A.; Kais, S. *J. Chem. Phys.* **2001**, *115*, 2621.

(19) Severson, M. W.; Buch, V. *J. Chem. Phys.* **1999**, *111*, 10866.

(20) Lee, J. Y.; Kim, J.; Lee, H. M.; Tarakeshwar, P.; Kim, K. S. *J. Chem. Phys.* **2000**, *113*, 6160.

(21) David, C. W. *J. Chem. Phys.* **1980**, *73*, 5395.

(22) Stillinger, F. H.; David, C. W. *J. Chem. Phys.* **1980**, *73*, 3384.

(23) Tsai, C. J.; Jordan, K. D. *J. Chem. Phys.* **1991**, *95*, 3850.

(24) Farantos, S. C.; Kapetanakis, S.; Vegiri, A. *J. Phys. Chem.* **1993**, *97*, 12158.

(25) Pedulla, J. M.; Jordan, K. D. *Chem. Phys.* **1998**, *239*, 593.

(26) Vegiri, A.; Farantos, S. C. *J. Chem. Phys.* **1993**, *98*, 4059.

(27) Rodriguez, J.; Laria, D.; Marceca, E. J.; Estrin, D. A. *J. Chem. Phys.* **1999**, *110*, 9039.

(28) Guevenc, Z. B.; Anderson, M. A. *Z. Phys. D: At., Mol. Clusters* **1996**, *36*, 171.

(29) Calvo, F.; Neirotti, J. P.; Freeman, D. L.; Doll, J. D. *J. Chem. Phys.* **2000**, *112*, 10350.

(30) Geyer, J. C. *Computing Science and Statistics: Proceedings of the 23rd Symposium on the Interface*; J. Am. Stat. Assoc.: New York, 1991; p 156.

(31) Marinari, E.; Parisi, G.; Ruiz-Lorenzo, *J.* Spin Glasses and Random Fields. In *Directions in Cond. Matter*; Young, A., Ed.; World Scientific: Singapore, 1998.

(32) Lynden-Bell, R. M.; Wales, D. J. *J. Chem. Phys.* **1994**, *101*, 1460.

(33) Jorgensen, W. L.; Chandrasekhar, J.; Madura, J. D.; Impey, R. W.; Klein, M. L. *J. Chem. Phys.* **1983**, *79*, 926.

(34) Allen, M. P.; Tilesday, D. J. *Computer Simulations of Liquids*; Oxford University Press: New York, 1987.

(35) Munro, L.; Tharrington, A.; Jordan, K. D. *Comput. Phys. Comm.* **2002**, *45*, 1.

(36) Frantz, D. D.; Doll, J. D. *J. Chem. Phys.* **1990**, *93*, 2769.

(37) Etters, R. D.; Kaelberer, J. B. *J. Chem. Phys.* **1977**, *66*, 5112.

(38) Stillinger, F. H.; Weber, T. A. *Science* **1984**, *225*, 983.

(39) Stone, A. J.; Dullweber, A.; Engvist, O.; Fraschini, E.; Hodges, M. P.; Meredith, A. W.; Popelier, P. L. A.; Wales, D. J. Orient: A program for studying interactions between molecules, version 3, inquiries to A. J. Stone, ajs@cam.ac.uk, 2000.

(40) Tsai, C.-J. *Theoretical characterization of small argon and water clusters*, Ph.D. Thesis in Department of Chemistry, 1992, University of Pittsburgh, Pittsburgh, PA.